




Effect of electromagnetic boundary conditions on the onset of small-scale dynamos driven by convection

M. Fontana ^{*}, P. D. Mininni , and P. Dmitruk 

*Universidad de Buenos Aires, Facultad de Ciencias Exactas y Naturales,
Departamento de Física, Ciudad Universitaria, 1428 Buenos Aires, Argentina
and CONICET - Universidad de Buenos Aires, Instituto de Física del Plasma (INFIP),
Ciudad Universitaria, 1428 Buenos Aires, Argentina*



(Received 7 July 2022; accepted 13 February 2023; published 1 March 2023)

We present a high-order numerical study of the dependence of the dynamo onset on electromagnetic boundary conditions in convecting Boussinesq flows forced by temperature gradients. Perfectly conducting boundaries, vacuum, and mixed boundary conditions are considered, treating fields and boundary conditions with close to spectral accuracy. Having one or two conducting boundaries greatly facilitates dynamo action. For the mixed case it is shown that the critical magnetic Reynolds number becomes independent of the Rayleigh number Ra for sufficiently large Ra .

DOI: [10.1103/PhysRevFluids.8.L031801](https://doi.org/10.1103/PhysRevFluids.8.L031801)

I. INTRODUCTION

Magnetic fields are ubiquitous in nature, defining the dynamics of many physical systems from the atomic to the galactic scale. Of particular interest is the mechanism by which magnetic fields are amplified inside celestial objects, such as the earth or the sun, to name two examples. The commonly accepted explanation for said origin is the transformation of kinetic into magnetic energy in an electrically conducting fluid inside the object, i.e., a magnetohydrodynamic (MHD) dynamo [1–5]. In the earth the mechanism that drives the flow is thought to be thermochemical convection due to interior cooling [6,7], while in the sun convection drives the small-scale dynamo responsible for the magnetic carpet [8].

Although the dynamo mechanism was first proposed at the beginning of the 20th century, it was quickly realized that simple symmetric flows are unable to sustain the magnetic fields observed in nature [9,10]. This notably increases experimental and numerical difficulties in reproducing dynamo generation [11–15]. Only in the last two decades laboratory experiments and simulations attained dynamos which exhibit features found in celestial magnetic fields, such as a high degree of symmetry, reversals, or periodic modulation [16–18]. The task of experimentally obtaining a self-sustaining dynamo from flow conditions which more closely resemble those found in celestial bodies is still being actively pursued [19–22].

Electromagnetic boundary conditions are known to affect the feasibility of attaining self-sustaining dynamos at fixed power input, together with domain geometry, forcing mechanisms, and fluid transport coefficients [23–28]. It was recently shown for rotating convective dynamos [29] that replacing insulating surroundings with perfect conductors greatly affects magnetic topology [30]. However, numerically studying different boundary conditions on equal footing, with the same numerical convergence, provides a challenge. The best confirmation of the influence of electromagnetic boundary conditions on dynamo feasibility is given by the Von-Kármán Sodium

*mfontana@df.uba.ar

(VKS) experiment [17]. In this liquid sodium experiment it was shown that changing propellers from stainless steel to iron resulted in measurable differences on the threshold for magnetic amplification.

In this letter we present a study of the influence of electromagnetic boundary conditions on the minimum magnetic Reynolds number required for dynamo action on convecting flows forced by temperature gradients. Direct numerical simulations (DNSs) of the three-dimensional (3D) nonlinear MHD equations are employed, using a method which guarantees quasi-spectral convergence for several types of boundary conditions while enforcing solenoidal magnetic fields to machine precision in nontrivial geometries [31,32]. Perfectly conducting or vacuum boundary conditions are considered, together with a combination of both.

II. GOVERNING EQUATIONS

We consider a magnetofluid in a rectangular domain with dimensions $L_x \times L_y \times L_z = (2\pi \times 2\pi \times 1)L_0$, where L_0 is a unitary length. The domain is periodic in the \hat{x} and \hat{y} directions and has impermeable no-slip isothermic walls at $z/L_0 = 0$ and 1. Gravity points in the $-\hat{z}$ direction. The dynamics is described under the Boussinesq approximation by the incompressible MHD equations,

$$\frac{\partial \mathbf{u}}{\partial t} + (\mathbf{u} \cdot \nabla) \mathbf{u} = -\nabla p + \gamma \theta \hat{z} + (\nabla \times \mathbf{b}) \times \mathbf{b} + \nu \nabla^2 \mathbf{u}, \quad \nabla \cdot \mathbf{u} = 0, \quad (1)$$

$$\frac{\partial \mathbf{b}}{\partial t} = \nabla \times (\mathbf{u} \times \mathbf{b}) + \eta \nabla^2 \mathbf{b}, \quad \nabla \cdot \mathbf{b} = 0, \quad (2)$$

$$\frac{\partial \theta}{\partial t} + (\mathbf{u} \cdot \nabla) \theta = \gamma u_z + \kappa \nabla^2 \theta, \quad (3)$$

with mechanical and thermal boundary conditions $\mathbf{u} = \mathbf{0}$, $\theta = 0$ at $z/L_0 = 0$ and 1. Here, \mathbf{u} , \mathbf{b} , and θ are the velocity, magnetic, and temperature fluctuations; ν , η , and κ are momentum, magnetic, and temperature diffusivities. The parameter γ controls the intensity of the buoyancy, which relates to the temperature difference between the plates ΔT as $\gamma = \sqrt{\alpha \Delta T} g / L_z$, with α the thermal expansion coefficient and g the gravity. The temperature fluctuation is the difference between the total fluid temperature T and the linear profile of the conductive solution T_0 , $T' = T - T_0$, which is expressed in velocity units as $\theta = \gamma L_z T' / \Delta T$ [31]. The magnetic field is expressed in velocity units as $\mathbf{b} = \mathbf{B} / \sqrt{\mu \rho}$, with \mathbf{B} the magnetic field, μ the permeability, and ρ the mean fluid density.

A set of parameters to describe Eqs. (1)–(3) is given by the kinematic Reynolds number Re , the magnetic Reynolds number Rm , the Rayleigh number Ra , and the thermal and magnetic Prandtl numbers Pr and Pm [31,33,34]. They can be expressed in terms of dimensional quantities as

$$Re = \frac{UL}{\nu}, \quad Rm = \frac{UL}{\eta}, \quad Ra = \frac{\gamma^2 L^4}{\nu \kappa}, \quad Pr = \frac{\kappa}{\nu}, \quad Pm = \frac{\eta}{\nu}, \quad (4)$$

with U and L the characteristic speeds and length scales. We consider U as the rms flow speed, $L = L_z/2$, and L_z/U as the unit of time. Re is the ratio between momentum advection and diffusion. Rm measures the ratio of magnetic induction to dissipation. Ra is the ratio of thermal diffusion time to the time of a fluid element freely ascending due to buoyancy. Finally, Pr and Pm compare the momentum diffusion time against the diffusive time scale of the temperature and magnetic fields.

We consider three scenarios for the electromagnetic boundaries: perfectly conducting walls at $z/L_0 = 0$ and 1, vacuum surroundings, and their combination. These conditions are of interest for different situations in geodynamos and stellar dynamos, and for laboratory experiments [17,18,35]. In the first case, perfectly conducting walls approximate the inner-to-outer earth core boundary [36]. In that case there can be no magnetic flux nor tangential electric field at the walls [37]. This implies the following relations at either $z/L_0 = 0$ or 1 (or at both boundaries):

$$\mathbf{j} \times \hat{z} = \mathbf{0}, \quad \partial_t \mathbf{b} \cdot \hat{z} = 0, \quad (5)$$

where $\mathbf{j} = \nabla \times \mathbf{b}$ is the current density, which at the boundary is proportional to the electric field \mathbf{E} if the walls are stationary. Vacuum surroundings approximate the scenario found in stars, and resemble insulating properties of the earth boundary between the outer core and the mantle [6]. If the fluid electrical permittivity is close to that of vacuum, they require the continuity of the magnetic field at the walls, together with the continuity of the normal electric field [37]. More precisely, the conditions

$$[\mathbf{b}] = \mathbf{0}, \quad [E_z] = 0, \quad (6)$$

must be obeyed at $z/L_0 = 0$ or 1 (or at both places). Here $[\]$ denotes the jump at the boundary. As vacuum surrounds the magnetofluid, the magnetic field in the box exterior must be compatible with a potential representation, as there are no currents there. Equation 6 requires the enforcement of this condition for \mathbf{b} at the walls. Finally, the mixed or combined case corresponds to one boundary condition (e.g., perfect conductor) at $z/L_0 = 0$, and the other boundary condition (e.g., vacuum surroundings) at $z/L_0 = 1$. Besides its relevance for the geodynamo, there are experiments which seek to obtain self-sustaining dynamos employing similar conditions [20,21].

A self-sustaining dynamo must amplify a seed magnetic field, increasing the magnetic energy of the system E^b as long as the flow is maintained or until nonlinear saturation is reached. For systems at finite magnetic Reynolds number, this implies that magnetic induction must overcome Ohmic losses. To study dynamo feasibility for a given Rm and geometry, it is common practice to consider the flow to be known, and an initial magnetic energy much smaller than the kinetic one, E^u , leading to the kinematic dynamo problem. A common strategy to study this problem theoretically is to neglect the feedback of the magnetic field on the velocity, and thus the equation for the magnetic field becomes a linear eigenvalue problem [5,7,38,39]. Correspondingly, to leading order

$$E^b(t) \propto e^{\sigma t}, \quad (7)$$

with σ the fastest growing (or slowest decaying) eigenvalue. When $\sigma > 0$ Eq. (7) only holds for a finite range of time, after which the decoupling of the induction equation stops being appropriate. The critical magnetic Reynolds number of dynamo onset Rm^{crit} is defined by $\sigma(Rm^{\text{crit}}) = 0$, and can be determined numerically by solving the MHD equations for a small enough random magnetic seed and for a large enough exploration of parameter space [23].

We consider the feasibility of self-sustaining convective dynamos employing DNSs of the full nonlinear Eqs. (1)–(3). Simulations are performed using the SPECTER parallel pseudo-spectral code [31,32], (available at Ref. [40]). Equations are evolved in time using a double-precision second-order Runge-Kutta method. SPECTER employs standard Fourier decompositions along periodic directions, attaining spectral convergence. Nonperiodic directions (\hat{z} in our case) utilize a Fourier continuation method with Gram polynomials (FC-Gram) [31,41], which allow high-order representation of boundary conditions without Gibbs degradation, and hence attain spectral accuracy inside the domain and high-order convergence at the boundaries. The absence of magnetic monopoles ($\nabla \cdot \mathbf{b} = 0$) is enforced to machine accuracy by evolving in time the vector potential \mathbf{a} in the Coulomb gauge, defined by $\nabla \times \mathbf{a} = \mathbf{b}$ and $\nabla \cdot \mathbf{a} = 0$. Particularly relevant for this study, SPECTER can implement different boundary conditions while retaining the aforementioned spectral convergence properties [32] (as a reference, typical errors are $\langle (\nabla \cdot \mathbf{b})^2 \rangle < 10^{-30}$, while quadratic errors in magnetic boundary conditions are $O(10^{-10})$ or smaller; vertical resolutions in the simulations were chosen to maintain small errors). Previous studies of convective dynamos, using other methods or simplified boundary conditions, can be found in Refs. [28,42–45]. For details of the method used here, or for the full implementation of the electromagnetic boundaries, see Ref. [32].

III. ROLE OF BOUNDARY CONDITIONS AT FIXED RAYLEIGH NUMBER

We first consider 19 simulations at fixed values of Ra and Re , with different magnetic Reynolds numbers and electromagnetic boundaries. We label simulations using Rm , even though Pm also changes. As we are interested in the regime in which both velocity and temperature fluctuations are

TABLE I. Simulations with $256 \times 256 \times 103$ grid points and different boundary conditions. Run is the label for each simulation, with C, M, and V denoting conducting, mixed, and vacuum boundaries. Re and Rm are the kinetic and magnetic Reynolds numbers, and Pm is the magnetic Prandtl number. σ is the growth rate of the magnetic energy, with negative values corresponding to decaying solutions. All simulations have $Ra = 2.25 \times 10^6$, $Re = 6.06 \times 10^2$, and $Pr = 1$.

Run	Rm	Pm	σ	Run	Rm	Pm	σ
C1	2.43×10^2	4.00×10^{-1}	0.41	M1	1.21×10^2	2.00×10^{-1}	0.13
C2	1.21×10^2	2.00×10^{-1}	0.32	M2	6.06×10^1	1.00×10^{-1}	0.07
C3	6.06×10^1	1.00×10^{-1}	0.26	M3	2.42×10^1	4.00×10^{-2}	-0.01
C4	2.41×10^1	4.00×10^{-2}	0.19	M4	1.21×10^1	2.00×10^{-2}	-0.07
C5	1.20×10^1	2.00×10^{-2}	0.11	V1	6.06×10^2	1.00	0.40
C6	6.06	1.00×10^{-2}	0.05	V2	4.83×10^2	8.00×10^{-1}	0.25
C7	2.40	4.00×10^{-3}	0.03	V3	3.03×10^2	5.00×10^{-1}	0.01
C8	1.20	2.00×10^{-3}	-0.00	V4	2.41×10^2	4.00×10^{-1}	-0.07
C9	8.64×10^{-1}	1.43×10^{-3}	-0.08	V5	1.21×10^2	2.00×10^{-1}	-0.18
C10	6.06×10^{-1}	1.00×10^{-3}	-0.32				

dynamically relevant at all scales, $Pr = 1$ is used. A summary of the runs is presented in Table I. Also, a rendering of temperature and magnetic field lines for a high-resolution run is shown in Fig. 1.

In the simulations we first integrate the nonmagnetic Boussinesq equations [Eqs. (1) and (3) with $\mathbf{b} = \mathbf{0}$] until a statistically steady turbulent convective state is attained. The value of Ra is picked to have rms flow speeds of order unity, with fields well resolved at the chosen spatial resolution. This state, together with an initial random magnetic field with energy 1×10^{-6} (six orders of magnitude smaller than the kinetic energy), is used as initial condition for the MHD simulations in Table I. They are integrated in time for each electromagnetic boundary (labeled “C” for conducting boundaries, “M” for mixed, and “V” for vacuum) and value of Rm, until a steady exponential growth or decay of the magnetic energy is attained.

In Fig. 2 the magnetic energy as a function of time is shown for all simulations. An exponential regime is attained in all cases (seen as linear trends in semilog scale). This is consistent with the fact that a kinematic dynamo should be recovered for small magnetic seeds. Moreover, for all electromagnetic boundaries both growing and decaying states are present. Note the profound effect of boundary conditions in the growth rate of magnetic energy and, by proxy, in the viability of a self-sustaining dynamo. Decaying solutions (denoted in the figure by discontinuous lines) are present in the vacuum case at values of Rm much larger than those for mixed boundaries or two

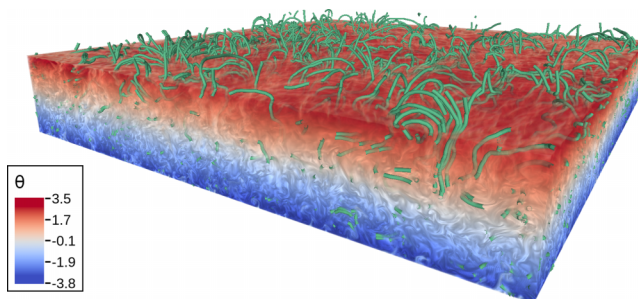


FIG. 1. Rendering using the software VAPOR [46,47] of the temperature fluctuations θ inside the domain, together with the magnetic field lines (in green) for simulation M22 [48]. Note that the magnetic field permeates into the vacuum above $z = 1$.

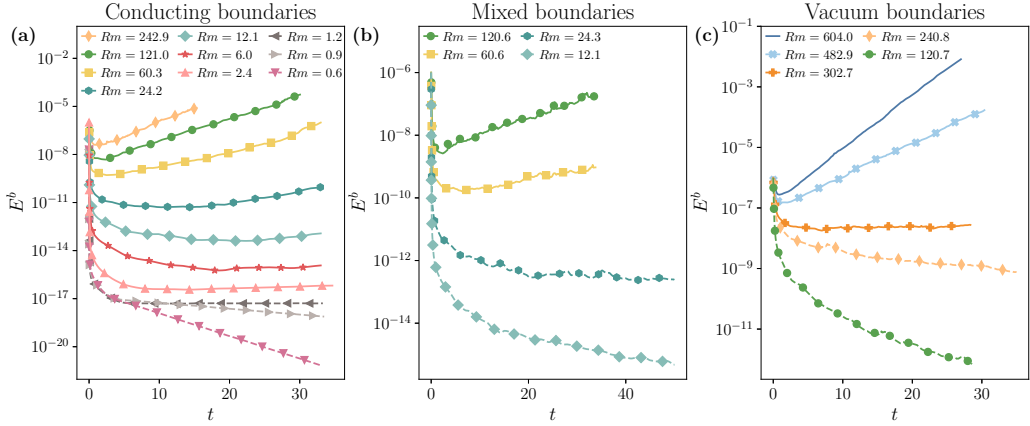


FIG. 2. Magnetic energy E^b as a function of time for all simulations at $Ra = 2.25 \times 10^6$. Line colors and markers denote the magnetic Reynolds number of each simulation. (a) The case of conducting boundaries, (b) mixed boundaries, and (c) vacuum surroundings. Simulations with decaying magnetic energy are drawn with discontinuous lines.

conducting plates. For the latter case Rm becomes so small in the nondynamo (decaying) solutions that E^b displays no fluctuations in time, becoming almost purely diffusive.

To characterize the behavior of the growth rate σ with Rm , we perform a least squares fit of the magnetic energy as a function of time in the range for which an exponential growth or decay can be observed. Results are presented in Fig. 3, where σ is shown as a function of Rm for all simulations. As in Fig. 2, there is a major difference for each boundary scenario in the value of Rm for which the zero crossing of σ is found. Critical values Rm^{crit} to have dynamo onset differ by more than an order of magnitude. For conducting plates $Rm^{\text{crit}} \approx 1.2$, whereas $Rm^{\text{crit}} \approx 30$ for mixed boundaries, and $Rm^{\text{crit}} \approx 303$ for vacuum.

To compare the energy-containing scales of the magnetic solutions, we compute the vertically averaged magnetic spectrum as a function of the horizontal wave number $k_{\parallel} = (k_x^2 + k_y^2)^{1/2}$, $\langle E^b(k_{\parallel}, z) \rangle_z$, and averaged across 10 turnover times. Note that *parallel* denotes the directions

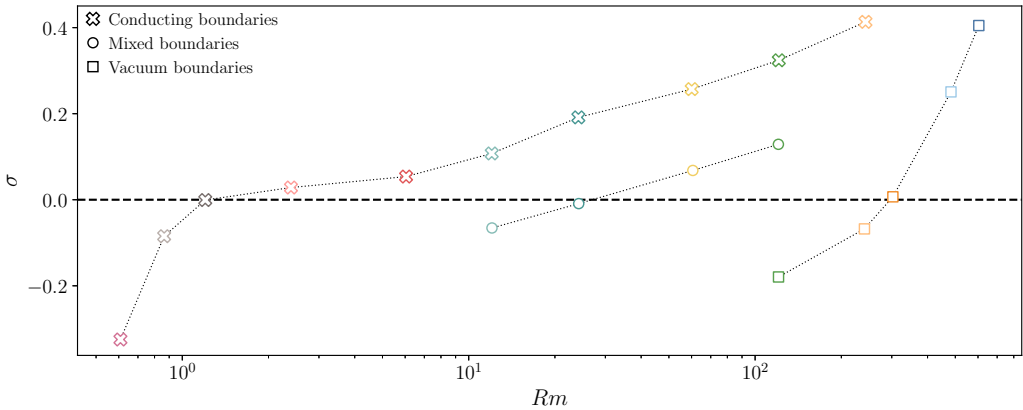


FIG. 3. Growth rate σ as a function of Rm for simulations with $Ra = 2.25 \times 10^6$. Markers denote electromagnetic boundary conditions: crosses for conducting boundaries, circles for mixed conditions, and squares for vacuum.

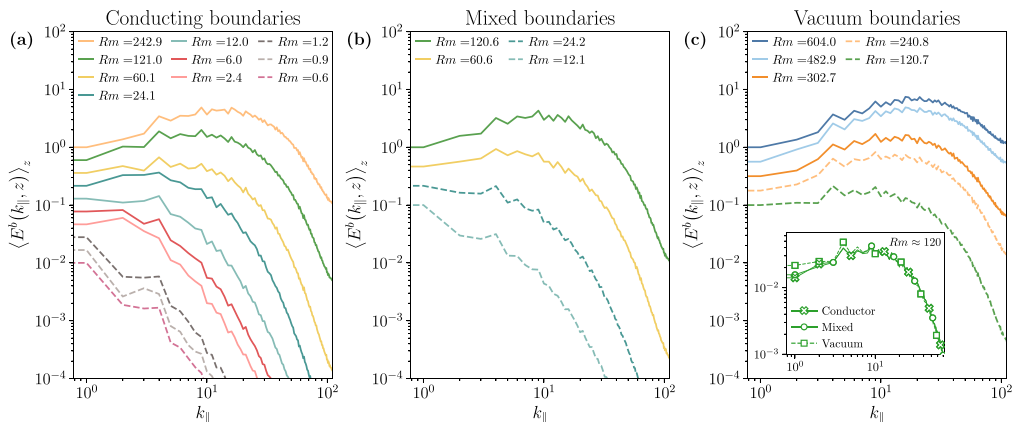


FIG. 4. Vertically averaged magnetic energy spectra $\langle E^b(k_{\parallel}, z) \rangle_z$ for wave numbers parallel to the wall, k_{\parallel} . (a) Magnetic spectra for conducting boundaries. (b) Same for mixed and for (c) vacuum boundaries. Decaying solutions are marked with dashes, and colors and symbols reference different values of Rm ($Ra = 2.25 \times 10^6$ in all cases). The inset in (c) shows normalized spectra for three simulations at the same Rm differing on boundary conditions (runs C2, M1, and V5). Wave numbers use $L_x = L_y = 2\pi L_0$ as the reference length. The correlation length of the velocity is similar in \hat{x} , \hat{y} , and \hat{z} , and is $\sim 0.6L_0$ for u_z , and $\ell_{\parallel} \approx 0.75L_0$ (in \hat{x} and \hat{y}) and $\ell_z \approx 0.5L_0$ for u_x and u_y .

tangential to the walls, and that the exponential growth or decay is removed before averaging in time by normalizing each spectra by its instantaneous magnetic energy. The result is shown in Fig. 4. All self-sustaining dynamo solutions generate magnetic fields with energy concentrated at intermediate or small scales, i.e., the dynamo is a small-scale dynamo. This is expected for flows with negligible helicity [1,10,49]. As Rm diminishes (i.e., as Ohmic diffusion increases), energy-containing structures shift to lower wave numbers. This can be appreciated in the spectra for all scenarios. For conducting walls, decaying solutions are obtained only when the diffusive scale is approximately the box length, for $Rm \leq 1$. This can be seen in Fig. 4, where a sharp decrease in $\langle E^b(k_{\parallel}, z) \rangle_z$ for $k_{\parallel} = 2$ (i.e., the second smallest wave number) characterizes solutions incompatible with self-sustaining dynamos. For mixed and vacuum boundary conditions no such behavior is seen in the spectra for $Rm \approx Rm^{\text{crit}}$. Finally, in all cases the spectra grow in a self-similar way: all wave numbers grow with the same rate.

Another interesting observation is found when comparing spectra (normalized by total energy) of the magnetic energy for flows operating at the same Re and Rm but with different boundary conditions. [This comparison is shown in the inset in Fig. 4(c)]. A clear contrast between scenarios exhibiting self-sustained dynamos (i.e., with conducting or mixed boundaries) and the magnetic extinction case (vacuum) is appreciated. While the three present a considerable accumulation of energy at intermediate scales, the latter has more energy at lower wave numbers.

IV. ROLE OF THE RAYLEIGH NUMBER

We now study the dependence of Rm^{crit} on convection strength. To this end we simulate the flow for varying values of Rm as Ra (and hence Re) increases. Note that increasing Ra requires finer grids. Table II lists the simulations with increased values of Ra . In all cases the time evolution of the magnetic energy still presents a short transient, after which it displays exponential growth or decay. Figure 5(a) shows σ as a function of Ra and Rm . For clarity, only the mixed scenario is shown; analogous results are obtained for purely conducting and vacuum boundaries. For fixed Ra , lower values of Rm correspond to lower or negative growth rates. More importantly, for fixed Rm the growth rate decreases as Ra increases. This is particularly relevant as naturally occurring dynamos

TABLE II. Simulations with increased values for Ra. Run lists the label for each simulation. $N_x \times N_y \times N_z$ indicates the spatial resolution, Ra is the Rayleigh number, Re and Rm are the kinetic and magnetic Reynolds numbers, Pm is the magnetic Prandtl number, and σ is the growth rate for the magnetic energy, with negative values corresponding to decaying solutions. All simulations have $\text{Pr} = 1$.

Run	$N_x \times N_y \times N_z$	Ra	Re	Rm	Pm	σ
C11	$512 \times 512 \times 231$	9.00×10^6	1.16×10^3	1.16×10^1	1.00×10^{-2}	0.009
C12	$512 \times 512 \times 231$	9.00×10^6	1.16×10^3	5.81	5.00×10^{-3}	-0.011
C13	$512 \times 512 \times 231$	9.00×10^6	1.16×10^3	2.32	2.00×10^{-3}	-0.195
C14	$512 \times 512 \times 231$	9.00×10^6	1.16×10^3	1.16	1.00×10^{-3}	-0.353
C21	$1024 \times 1024 \times 487$	3.60×10^7	2.25×10^3	1.12×10^1	5.00×10^{-3}	-0.029
M11	$512 \times 512 \times 231$	9.00×10^6	1.16×10^3	2.91×10^2	2.50×10^{-1}	0.527
M12	$512 \times 512 \times 231$	9.00×10^6	1.15×10^3	1.15×10^2	1.00×10^{-1}	0.012
M13	$512 \times 512 \times 231$	9.00×10^6	1.16×10^3	5.80×10^1	5.00×10^{-2}	-0.023
M14	$512 \times 512 \times 231$	9.00×10^6	1.16×10^3	2.32×10^1	2.00×10^{-2}	-0.135
M21	$1024 \times 1024 \times 487$	3.60×10^7	2.25×10^3	2.81×10^2	1.25×10^{-1}	0.329
M22	$1024 \times 1024 \times 487$	3.60×10^7	2.24×10^3	1.12×10^2	5.00×10^{-2}	0.036
M23	$1024 \times 1024 \times 487$	3.60×10^7	2.25×10^3	5.62×10^1	2.50×10^{-2}	-0.072
V11	$512 \times 512 \times 231$	9.00×10^6	1.14×10^3	5.68×10^2	5.00×10^{-1}	0.029
V12	$512 \times 512 \times 231$	9.00×10^6	1.16×10^3	2.33×10^2	2.00×10^{-1}	-0.100
V21	$1024 \times 1024 \times 487$	3.60×10^7	2.23×10^3	5.57×10^2	2.50×10^{-1}	-0.112
V22	$1024 \times 1024 \times 487$	3.60×10^7	2.25×10^3	2.25×10^2	1.00×10^{-1}	-0.212

operate at extreme values of Ra (of order 1×10^{20} or higher [50]). Consequently, a determination of asymptotic values of Rm^{crit} for large Ra would provide better constraints than those in Fig. 3.

To better analyze this effect we study the behavior of Rm^{crit} as a function of Ra. To obtain a value for Rm^{crit} we pick, for each value of Ra, the two simulations with growth/decay rates closer to zero. We then estimate a linear relation for $\sigma(Rm)$ between those values and obtain Rm^{crit} from its root. The result is shown in Fig. 5(b). Rm^{crit} first grows with Ra, and for the mixed case it

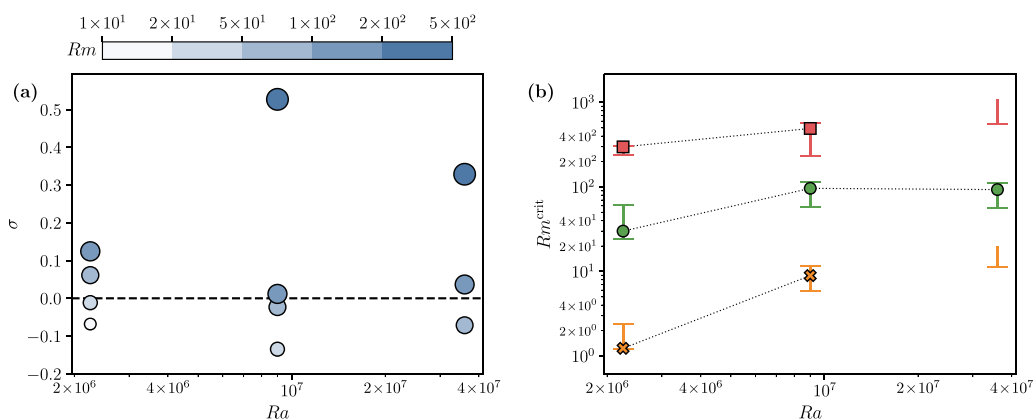


FIG. 5. (a) Growth rate of the magnetic energy σ as a function of the Rayleigh number Ra, for mixed boundaries. Increasing values of Rm are denoted with a darker shade and bigger markers. (b) Critical magnetic Reynolds number Rm^{crit} as a function of Ra. Error bars denote the Rm values corresponding to the pair of simulations whose growth rates are closer to zero, and filled symbols correspond to Rm^{crit} obtained from a linear interpolation of $\sigma(Rm)$ between those values. Labels for filled symbols are as in Fig. 3, and open error bars denote lower bounds for Rm^{crit} .

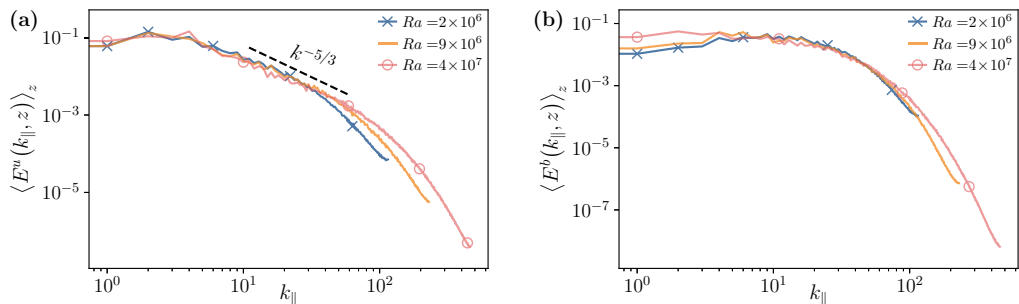


FIG. 6. Vertically averaged energy spectra $\langle E(k_{\parallel}, z) \rangle_z$ as a function of k_{\parallel} for simulations M4 (blue with crosses), M12 (orange), and M22 (red with empty circles), which operate at approximately the same Rm. (a) Kinetic energy spectrum E^u , and (b) magnetic energy spectrum E^b . Spectra are normalized by their total energy.

seems to saturate and remain of $O(10^2)$ even when Ra is increased fourfold. This suggests a finite asymptotic value for Rm^{crit} as $Ra \rightarrow \infty$, as suggested in Ref. [51] using other methods. The order of magnitude is compatible with results for the same boundary conditions [52]. In the conducting and vacuum scenarios only decaying solutions are available at the highest value of Ra for the values of Rm explored. Thus, only a lower bound for Rm^{crit} is marked in the figure. However, simulation C21 has a small $\sigma \lesssim 0$, and Rm^{crit} can accordingly be expected to be $O(10)$, while simulations V21 and V22 have smaller σ , which suggest $Rm^{\text{crit}} \sim O(10^3)$ (see Table II). Thus, at least in the range of Ra considered, Rm^{crit} differs for the different boundary conditions.

Finally, we consider the effect Ra has on the kinetic and magnetic energy spectra. These are shown for runs M4, M12, and M22 (with different Ra but similar Rm) in Fig. 6. In all cases the spectra are well resolved. In Fig. 6(a) the kinetic energy content at the largest scales is basically indistinguishable among all simulations. The spectral slope at intermediate scales is similar in all cases, with a power spectrum compatible with $k_{\parallel}^{-5/3}$ that extends to larger values of k_{\parallel} as Ra grows. Indeed, it can be readily seen that the kinetic spectrum gets wider as Ra increases. Contrary to the kinetic energy spectra, the width of the magnetic spectra remains the same when Ra increases, as shown in Fig. 6(b). This is to be expected, as the magnetic Reynolds number is similar for the three simulations. Conversely, the largest scales seem to be more disparate, containing a greater amount of magnetic energy as Ra increases. This indicates that for larger values of Ra magnetic energy grows at slightly larger scales, albeit at a smaller rate.

V. DISCUSSION

We studied the problem of attaining dynamos in a channel filled with a conducting fluid undergoing Rayleigh-Bénard convection. To this purpose we performed multiple DNSs of the Boussinesq approximation to the MHD equations, utilizing a versatile numerical method with quasi-spectral convergence [32]. We analyzed the growth or decay of an initially small random magnetic field as a function of time, determining the critical magnetic Reynolds number for which self-sustaining dynamo action becomes feasible for three electromagnetic boundary conditions at the floor and the top of the channel and for different values of Ra.

Boundary effects are particularly relevant, as laboratory experiments have shown strong sensitivity of the dynamo onset to the electromagnetic properties of the containing vessel and the propellers. For the convective case, we analyzed dynamo feasibility for three sets of boundary conditions: both plates perfectly conducting, both walls surrounded by vacuum (with a potential magnetic field outside the domain), and a combination of a conducting floor with vacuum outside the top of the channel. In all cases the magnetic energy was observed to grow or decrease exponentially in time,

allowing for the determination of growth or decay rates, and of critical values for dynamo action. Sharp differences, of one order of magnitude or more, were observed in Rm^{crit} for each set of boundary conditions, with the fully conducting case showing the mildest constraint and the entirely vacuum scenario displaying the most severe restriction. Consistent with experiments, utilizing conducting materials seems to be notably advantageous for self-sustaining dynamos. Modifying boundary conditions changes the regions of accumulation of magnetic energy: near the walls and with less dissipation for the perfect conductor, and in the bulk with more dissipation for vacuum surroundings.

Raising the strength of convection and turbulence results in a growth of Rm^{crit} . The observed effect seems to asymptote to values of Rm^{crit} independent of Ra for the mixed case, and for all values of Ra explored Rm^{crit} differs for the three boundaries considered. In all cases dynamos generate magnetic fields at intermediate scales, with magnetic energy spectra that peak at scales smaller than the flow integral scale.

ACKNOWLEDGMENTS

The authors acknowledge support from CONICET and ANPCyT through PIP, Argentina Grant No. 11220150100324CO, and PICT, Argentina Grant No. 2018-4298. We also thank the Physics Department at the University of Buenos Aires for providing computing time on its Dirac cluster.

-
- [1] A. Pouquet, U. Frisch, and J. Léorat, Strong MHD helical turbulence and the nonlinear dynamo effect, *J. Fluid Mech.* **77**, 321 (1976).
 - [2] A. Brandenburg and K. Subramanian, Astrophysical magnetic fields and nonlinear dynamo theory, *Phys. Rep.* **417**, 1 (2005).
 - [3] G. Verhille, N. Plihon, M. Bourgoïn, P. Odier, and J.-F. Pinton, Laboratory dynamo experiments, *Space Sci. Rev.* **152**, 543 (2010).
 - [4] S. Tobias, The turbulent dynamo, *J. Fluid Mech.* **912**, P1 (2021).
 - [5] P. M. Mannix, Y. Ponty, and F. Marcotte, Systematic Route to Subcritical Dynamo Branches, *Phys. Rev. Lett.* **129**, 024502 (2022).
 - [6] C. A. Jones, 8.05 - thermal and compositional convection in the outer core, in *Treatise on Geophysics*, edited by G. Schubert (Elsevier, Amsterdam, 2007), pp. 131–185.
 - [7] P. H. Roberts and E. M. King, On the genesis of the Earth’s magnetism, *Rep. Prog. Phys.* **76**, 096801 (2013).
 - [8] I. N. Kitiashvili, A. G. Kosovichev, N. N. Mansour, and A. A. Wray, Realistic modeling of local dynamo processes on the Sun, *Astrophys. J.* **809**, 84 (2015).
 - [9] T. G. Cowling, The magnetic field of sunspots, *Mon. Not. R. Astron. Soc.* **94**, 39 (1933).
 - [10] F. Krause and K. H. Radler, *Mean-Field Magnetohydrodynamics and Dynamo Theory* (Pergamon, New York, 1980).
 - [11] A. Gailitis, O. Lielausis, S. Dement’ev, E. Platācis, A. Ciferšons, G. Gerbeth, T. Gundrum, F. Stefani, M. Christen, H. Hänel, and G. Will, Detection of a Flow Induced Magnetic Field Eigenmode in the Riga Dynamo Facility, *Phys. Rev. Lett.* **84**, 4365 (2000).
 - [12] U. Müller and R. Stieglitz, The Karlsruhe dynamo experiment, *Nonlinear Processes Geophys.* **9**, 165 (2002).
 - [13] M. D. Nornberg, E. J. Spence, R. D. Kendrick, C. M. Jacobson, and C. B. Forest, Intermittent Magnetic Field Excitation by a Turbulent Flow of Liquid Sodium, *Phys. Rev. Lett.* **97**, 044503 (2006).
 - [14] N. Schaeffer, D. Jault, H.-C. Nataf, and A. Fournier, Turbulent geodynamo simulations: A leap towards Earth’s core, *Geophys. J. Int.* **211**, 1 (2017).
 - [15] M. Fontana, P. D. Mininni, and P. Dmitruk, Magnetic structure, dipole reversals, and $1/f$ noise in resistive MHD spherical dynamos, *Phys. Rev. Fluids* **3**, 123702 (2018).

- [16] G. A. Glatzmaiers and P. Roberts, A three-dimensional self-consistent computer simulation of a geomagnetic field reversal, *Nature (London)* **377**, 203 (1995).
- [17] R. Monchaux, M. Berhanu, S. Aumaître, A. Chiffaudel, F. Daviaud, B. Dubrulle, F. Ravelet, S. Fauve, N. Mordant, F. Pétrélis, M. Bourgoin, P. Odier, J. Pinton, N. Plihon, and R. Volk, The von Kármán Sodium experiment: Turbulent dynamical dynamos, *Phys. Fluids* **21**, 035108 (2009).
- [18] M. Berhanu, G. Verhille, J. Boisson, B. Gallet, C. Gissinger, S. Fauve, N. Mordant, F. Pétrélis, M. Bourgoin, P. Odier, J. F. Pinton, N. Plihon, S. Aumaître, A. Chiffaudel, F. Daviaud, B. Dubrulle, and C. Pirat, Dynamo regimes and transitions in the VKS experiment, *Eur. Phys. J. B* **77**, 459 (2010).
- [19] P. Olson, Experimental dynamos and the dynamics of planetary cores, *Annu. Rev. Earth Planet Sci.* **41**, 153 (2013).
- [20] C. M. Cooper, J. Wallace, M. Brookhart, M. Clark, C. Collins, W. X. Ding, K. Flanagan, I. Khalzov, Y. Li, J. Milhone, M. Nornberg, P. Nonn, D. Weisberg, D. G. Whyte, E. Zweibel, and C. B. Forest, The Madison plasma dynamo experiment: A facility for studying laboratory plasma astrophysics, *Phys. Plasmas* **21**, 013505 (2014).
- [21] D. S. Zimmerman, S. A. Triana, H. C. Nataf, and D. P. Lathrop, A turbulent, high magnetic Reynolds number experimental model of Earth's core, *J. Geophys. Res.: Solid Earth* **119**, 4538 (2014).
- [22] R. E. Rojas, A. Perevalov, T. Zürner, and D. P. Lathrop, Experimental study of rough spherical Couette flows: Increasing helicity toward a dynamo state, *Phys. Rev. Fluids* **6**, 033801 (2021).
- [23] Y. Ponty, P. D. Mininni, D. C. Montgomery, J. F. Pinton, H. Politano, and A. Pouquet, Numerical Study of Dynamo Action at Low Magnetic Prandtl Numbers, *Phys. Rev. Lett.* **94**, 164502 (2005).
- [24] A. A. Schekochihin, N. E. L. Haugen, A. Brandenburg, S. C. Cowley, J. L. Maron, and J. C. McWilliams, The onset of a small-scale turbulent dynamo at low magnetic Prandtl numbers, *Astrophys. J.* **625**, L115 (2005).
- [25] A. Jackson, A. Sheyko, P. Marti, A. Tilgner, D. Cébron, S. Vantieghem, R. Simitev, F. Busse, X. Zhan, G. Schubert, S. Takehiro, Y. Sasaki, Y.-Y. Hayashi, A. Ribeiro, C. Nore, and J.-L. Guermond, A spherical shell numerical dynamo benchmark with pseudo-vacuum magnetic boundary conditions, *Geophys. J. Int.* **196**, 712 (2014).
- [26] M. Sadek, A. Alexakis, and S. Fauve, Optimal Length Scale for a Turbulent Dynamo, *Phys. Rev. Lett.* **116**, 074501 (2016).
- [27] V. Skoutnev, J. Squire, and A. Bhattacharjee, Small-scale dynamo in stably stratified turbulence, *Astrophys. J.* **906**, 61 (2021).
- [28] J. Varela, S. Brun, B. Dubrulle, and C. Nore, Effects of turbulence, resistivity and boundary conditions on helicoidal flow collimation: Consequences for the Von-Kármán-Sodium dynamo experiment, *Phys. Plasmas* **24**, 053518 (2017).
- [29] M. Yan, S. Tobias, and M. Calkins, Scaling behaviour of small-scale dynamos driven by Rayleigh-Bénard convection, *J. Fluid Mech.* **915**, A15 (2021).
- [30] P. Kolhey, S. Stellmach, and D. Heyner, Influence of boundary conditions on rapidly rotating convection and its dynamo action in a plane fluid layer, *Phys. Rev. Fluids* **7**, 043502 (2022).
- [31] M. Fontana, O. Bruno, P. Mininni, and P. Dmitruk, Fourier continuation method for incompressible fluids with boundaries, *Comput. Phys. Commun.* **256**, 107482 (2020).
- [32] M. Fontana, P. D. Mininni, O. P. Bruno, and P. Dmitruk, Vector potential-based MHD solver for non-periodic flows using Fourier continuation expansions, *Comput. Phys. Commun.* **275**, 108304 (2022).
- [33] M. Meneguzzi and A. Pouquet, Turbulent dynamos driven by convection, *J. Fluid Mech.* **205**, 297 (1989).
- [34] C. A. Jones and P. H. Roberts, Convection-driven dynamos in a rotating plane layer, *J. Fluid Mech.* **404**, 311 (2000).
- [35] A. Gailitis, O. Lielausis, E. Platācis, G. Gerbeth, and F. Stefani, Colloquium: Laboratory experiments on hydromagnetic dynamos, *Rev. Mod. Phys.* **74**, 973 (2002).
- [36] J. Wicht, Inner-core conductivity in numerical dynamo simulations, *Phys. Earth Planet. Inter.* **132**, 281 (2002).
- [37] J. D. Jackson, *Classical Electrodynamics*, 2nd ed. (Wiley, New York, 1975).
- [38] K. Moffatt, *Magnetic Field Generation in Electrically Conducting Fluids* (Cambridge University Press, Cambridge, 1978).

- [39] P. Roberts and G. Glatzmaier, Geodynamo theory and simulations, *Rev. Mod. Phys.* **72**, 1081 (2000).
- [40] M. Fontana and P. D. Mininni, SPECTER (Special PERiodic Continuation Turbulence solver), <https://github.com/mfontanaar/SPECTER>.
- [41] O. P. Bruno and M. Lyon, High-order unconditionally stable FC-AD solvers for general smooth domains I. Basic elements, *J. Comput. Phys.* **229**, 2009 (2010).
- [42] J.-C. Thelen and F. Cattaneo, Dynamo action driven by convection: The influence of magnetic boundary conditions, *Mon. Not. R. Astron. Soc.* **315**, L13 (2000).
- [43] F. Cattaneo, T. Emonet, and N. Weiss, On the interaction between convection and magnetic fields, *Astrophys. J.* **588**, 1183 (2003).
- [44] L. Chen, W. Herreman, and A. Jackson, Optimal dynamo action by steady flows confined to a cube, *J. Fluid Mech.* **783**, 23 (2015).
- [45] M. R. Proctor, Energy requirement for a working dynamo, *Geophys. Astrophys. Fluid Dyn.* **109**, 611 (2015).
- [46] J. Clyne, P. Mininni, A. Norton, and M. Rast, Interactive desktop analysis of high resolution simulations: Application to turbulent plume dynamics and current sheet formation, *New J. Phys.* **9**, 301 (2007).
- [47] S. Li, S. Jaroszynski, S. Pearse, L. Orf, and J. Clyne, Vapor: A visualization package tailored to analyze simulation data in earth system science, *Atmosphere* **10**, 10.3390/atmos10090488 (2019).
- [48] See Supplemental Material at <http://link.aps.org/supplemental/10.1103/PhysRevFluids.8.L031801> for an animation of the convective dynamo.
- [49] A. A. Schekochihin, S. C. Cowley, S. F. Taylor, G. W. Hammett, J. L. Maron, and J. C. McWilliams, Saturated State of the Nonlinear Small-Scale Dynamo, *Phys. Rev. Lett.* **92**, 084504 (2004).
- [50] P. Olson, 8.01 - overview, in *Treatise on Geophysics*, edited by G. Schubert (Elsevier, Amsterdam, 2007), pp. 1–30.
- [51] J. Léorat, A. Pouquet, and U. Frisch, Fully developed MHD turbulence near critical magnetic Reynolds number, *J. Fluid Mech.* **104**, 419 (1981).
- [52] P. Bushby, B. Favier, M. Proctor, and N. Weiss, Convectively driven dynamo action in the quiet sun, *Geophys. Astrophys. Fluid Dyn.* **106**, 508 (2012).